Applied Catalysis B: Environmental 168-169 (2015) 25–32

Contents lists available at ScienceDirect

Applied Catalysis B: Environmental

journal homepage: www.elsevier.com/locate/apcatb

Dye-sensitized photoelectrochemical cell on plasmonic Ag/AgCl @ chiral TiO_2 nanofibers for treatment of urban wastewater effluents, with simultaneous production of hydrogen and electricity

Dawei Wang[a], Yi Li[a,*], Gianluca Li Puma[b,**], Chao Wang[a], Peifang Wang[a], Wenlong Zhang[a], Qing Wang[a]

[a] Key Laboratory of Integrated Regulation and Resource Development of Shallow Lakes, Ministry of Education, College of Environment, Hohai University, Xi Kang Road #1, Nanjing 210098, PR China
[b] Environmental Nanocatalysis & Photoreaction Engineering, Department of Chemical Engineering, Loughborough University, Loughborough LE11 3TU, United Kingdom

ARTICLE INFO

Article history:
Received 5 July 2014
Received in revised form 27 October 2014
Accepted 8 November 2014
Available online 4 December 2014

Keywords:
Wastewater treatment
Dye-sensitized photoelectrochemical cell
Hydrogen production
Electricity generation
Ag/AgCl @ chiral TiO_2 nanofibers

ABSTRACT

The feasibility of simultaneous production of hydrogen and electricity with simultaneous contaminants removal from "actual" urban wastewater within a dye-sensitized photoelectrochemical cell (DSPC) is demonstrated for the first time. The photoanode in the DSPC was a novel nanostructured plasmonic Ag/AgCl @ chiral TiO_2 nanofibers (Ag and AgCl nanoparticles supported on chiral TiO_2 nanofibers). The electrolyte in the DSPC was actual wastewater to which an estrogen (17-β-ethynylestradiol, EE2) and a heavy metal (Cu^{2+}) were added. The contaminants in the wastewater rather than I^-/I_3^- (usual electrolyte in conventional DSPCs) acted as electrons' bridges for the stabilization of charges in this DSPC. Almost total removal of total organic carbon (TOC), Cu^{2+}, EE2, and 70% removal of total nitrogen (TN) were achieved under visible-light irradiation. A relatively high solar energy conversion efficiency (PCE 3.09%) was recorded and approximately 98% of the electricity was converted to H_2 after the consumption of dissolved oxygen (DO), Cu^{2+} and TN. This performance was attributed to the "symbiotic" relationship between the TiO_2 chiral nanofibers and the plasmonic effect of Ag nanoparticles at the photoanode, although Ag may act as a recombination site which may hinder the generation of electricity. The dye N719 in this study exhibited a temporary sensitization effect, and a more efficient sensitizer is expected to be studied in the future. This study opens up new opportunities for producing renewable energy from wastewater treatment processes including organic and inorganic matter as viable resources.

1. Introduction

Energy crisis and increasing environmental pollution are two of the greatest threats to human population sustainability at a global scale. Within this wide contest, wastewater previously considered as a waste is increasingly being used as a valuable resource for producing fresh water, energy and fertilizing nutrients (N and P). For instance, the wastewater's organic content can be converted into methane gas through the anaerobic process [1], and microbial fuel cell (MFC) [2,3] may also be a viable route for the production of energy from wastewater treatment. Photocatalytic oxidation using titanium dioxide (TiO_2) is an effective method for the removal of chemically stable contaminants, it requires no chemicals input or output and TiO_2 is inexpensive and non-toxic [4–8]. The photocatalytic oxidation of contaminants is initiated by the excitation of TiO_2, which results in the promotion of an electron (e−) to the conduction band (CB) and creation of a hole (h+) in the valence band (VB) of TiO_2 [9]. The photogenerated electrons and holes produce highly reactive oxygen species (ROS) (*i.e.* H_2O_2, $HO\cdot$, $O_2\cdot^-$) which can attack and oxidize organic contaminants [10], ultimately leading to complete mineralization.

The utilization of freely available solar energy as the only energy input makes photocatalysis a sustainable and green process. However, one of the most important advancement in wastewater treatment should be the development of a new process that can simultaneously capture the chemical energy of the oxidized contaminants while meeting the effluent quality standards [1]. Although the appeal of the direct conversion of solar into chemical energy during a wastewater treatment process has been recognized

* Corresponding author. Tel.: +86 2583786251.
** Corresponding author. Tel.: +44 1509222510.
E-mail addresses: envly@hhu.edu.cn (Y. Li), g.lipuma@lboro.ac.uk (G. Li Puma).

http://dx.doi.org/10.1016/j.apcatb.2014.11.012
0926-3373/

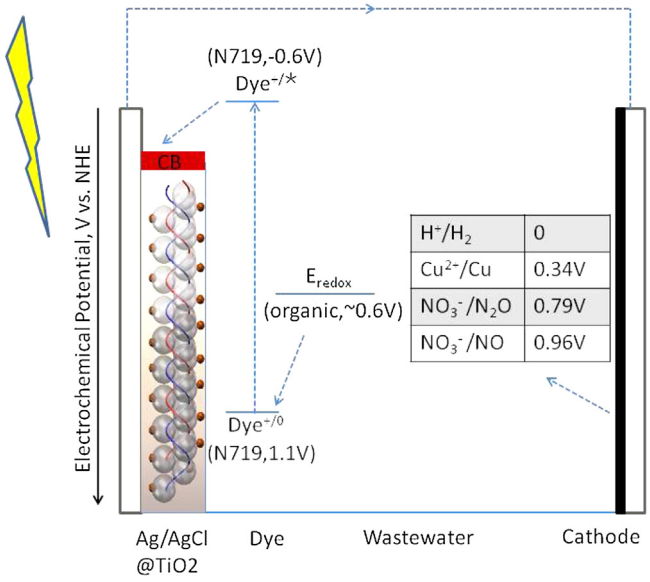

Fig. 1. Schematic diagram of the DSPC cell.

for a long time, effective efforts are still rare. Recently, a series of studies have succeeded in using some organic fractions in wastewater (*i.e.* phenolic compounds and dyes) to act as electron donors for producing H_2 [11,12] and for electricity generation [13], and our group has reported the feasibility of hydrogen generation during the removal of emerging contaminants [14,15]. Very few studies have focused on the harvesting of energy during the removal of both organic and inorganic compounds (*e.g.* nutrients) in contaminated water and wastewater, making this the main scientific and technological challenge for the water industry. In this study, inspired by the PhotoFuelCell system proposed by Lianos and coworkers [16–19], we demonstrate that dye-sensitized photoelectrochemical cells (DSPCs) may be valuable to address this technological issue.

The concept of DSPCs is similar with that of dye-sensitized solar cells (DSSCs). In a DSSC, the sensitizer, which is usually a dye, absorbs the incident photons resulting in the excitation of electrons from the highest occupied molecular orbital (HOMO) to the lowest unoccupied molecular orbital (LUMO) of the dye. The excited electrons are then injected to the conduction band (CB) of the photoanode material (usually TiO_2), they further transfer to the photoanode fluorine-doped tin oxide (FTO) supporting the TiO_2 and through the external load, travel to the cathode FTO and to the cathode material (usually a Pt layer). They then transfer to the HOMO of the redox couples (usually I^-/I_3^-), and finally back to the HOMO of the dye [20,21] to close the cycle. In this process, the redox couples play a very important role as electrons bridges for the stabilization of charges in the DSSCs. One major innovating aspect of the present study is the replacement of the redox couples (such as I^-/I_3^-) in DSSCs with organic and inorganic compounds naturally occurring in urban wastewater, which collectively can act as an effective electrolyte and also reduced the dye from an excited state to a stable state. Although dyes have been reported to be unstable in water, they may have a temporary sensitization effect. Under an ideal situation, organic contaminants may be oxidized by an excited dye in the photoanode, while nitrate and heavy metal could be reduced in the cathode (Fig. 1) including the reduction of protons to H_2.

In this study, the DSPC with Ag/AgCl @ chiral TiO_2 nanofibers as the photoanode material, a platinized FTO sheet as the counter electrode and actual urban wastewater as the electrolyte was investigated for the first time for the simultaneous generation of electricity, hydrogen gas and for the simultaneous removal of contaminants from wastewater, including 17-β-ethynylestradiol (EE2) as a representative of chemically stable and emerging contaminants, which was added to the wastewater. The performance and the underlying mechanisms of this highly innovating concept for environmental remediation with simultaneous generation of renewable energy are presented in this study.

2. Materials and methods

2.1. Synthesis of Ag/AgCl @ chiral TiO_2 nanofibers photoanode

Chiral TiO_2 nanofibers were synthesized with N-(1-oxooctadecyl)-D-glutamic acid (C_{18}-D-Glu) as template and details can be found in our previous study [22]. In a typical synthesis, C18-D-Glu (0.06 g, 0.16 mmol) was dissolved in a mixture of methanol (27.2 g) and deionized water (160 ml) while stirring at room temperature. After the mixture was stirred for 10 min, titanium diisopropoxide bis(acetylacetonate) (0.58 g, 75% in isopropanol, purchased from TCI) was added to the mixture with stirring at 55 °C. The mixture was allowed to react at 55 °C with stirring for 2 h. The products were collected by centrifugal separation and dried by freeze drying at −60 °C, which resulted in a pale yellow powder. All organics in this product were removed by calcination at 550 °C, and crystalline anatase was obtained.

Then, the as-prepared pure chiral TiO_2 nanofibers were used to fabricate Ag/AgCl @ chiral TiO_2 nanofibers. In a typical synthesis of Ag/AgCl @ chiral TiO_2 nanofibers, pure chiral TiO_2 nanofibers (0.2 g) and cetyltrimethylammonium chloride (0.3 g, purchased from TCI) were added into deionized water (100 mL) while stirring at room temperature. After the mixture was stirred for 60 min, $AgNO_3$ (2.0 mL, 0.1 M) was quickly added into the mixture. The resulting solution was stirred at room temperature for further 60 min and irradiated with an 8 W UVC light for 40 min. The suspension was collected by centrifugal separation and then dried at 80 °C for 8 h, which resulted in a brown powder. Finally, the powder was calcined at 300 °C in air and Ag/AgCl @ chiral TiO_2 nanofibers were obtained. Chiral TiO_2 nanofibers were also physically broken with the application of pressure at 10 MPa using FTIR tablet press (to avoid changes of the TiO_2 morphological structures) prior to the deposition of Ag/AgCl, to prepare Ag/AgCl @ broken chiral TiO_2 nanofibers. The synthesis of Ag/AgCl @ broken chiral TiO_2 nanofibers was carried out under the same conditions used to prepare the Ag/AgCl @ chiral TiO_2 nanofibers, to ensure that an equal amount of Ag/AgCl was deposited on the same amount of chiral TiO_2 nanofibers and broken chiral nanofibers.

2.2. Assembly of DSPCs

The Ag/AgCl @ chiral TiO_2 nanofibers photoanode was prepared by adding 6 g of polyvinyl alcohol (PVA) (MW 22,000, purchased from TCI) into 14 mL of boiled distilled water with powerful stirring, producing a highly viscous liquid that was further diluted by adding to a solvent made of 18 mL distilled water and 25 mL ethanol at 70 °C. Then, 1.62 g of the as-prepared Ag/AgCl @ chiral TiO_2 nanofibers were added into the PVA/water/ethanol solution to produce a suspension which was left to cool to room temperature. The photoanode films were produced on FTO glass (2.3 mm thickness, 25 cm^2 area, 8 Ω/sq, Dyesol Glass, previously cleaned with 2-propanol in an ultrasonic bath for 30 min, and then thoroughly rinsed with distilled water, followed by drying on nitrogen) by coating a paste of the suspension using the doctor-blade technique [23]. After coating the films were kept in a clean box for 15 min to relax surface irregularities and the residual mechanical stress of the coating. Finally, the photoanode was gradually heated at 80 °C for 15 min and then at 500 °C for 30 min. The thickness of

the film (11 μm) was increased by repeating this doctor-blade technique [24]. For the preparation of the counter electrode, a drop of 5 mM $H_2PtCl_6 \cdot H_2O$ in 2-propanol was placed on the FTO glass substrate (25 cm^2 area), following by drying and annealing at 450 °C for 30 min.

The photoanode was impregnated with the dye by immersion into a 1:1 (v/v) mixture of acetonitrile (CR, Sigma–Aldrich) and tert-butanol (CR, Sigma–Aldrich) containing a 0.5 mM N719 (Dyesol) dye solution for 6 h. Then, the dye-loaded photoanode was washed with acetonitrile and dried with nitrogen.

The DSPCs were assembled into a sandwich design using the dye loaded photoanode and the cathode. The distance between the two electrodes was 5 mm. The gap between the electrodes was filled with actual wastewater collected from the effluent of a municipal wastewater treatment plant in Suzhou (China) with further addition (0.56 mg/L) of 17-β-ethynylestradiol (EE2) (HPLC grade, Merck) and $CuSO_4$ (1.03 mg/L). The chemical properties of the wastewater effluent are presented in Table S1 (Supplementary Material). The pH of the wastewater in the DSPCs was adjusted using 1 mol/L H_2SO_4.

2.3. Instruments and experimental conditions

Scanning electron microscopy (SEM) images were obtained with a JEOL JSM-7041F at an accelerating voltage of 1 kV. Large scope EDX analysis was conducted on an energy dispersive X-ray spectrometer (ZAF Quantification) attached to the SEM of JEOL JSM-7041F. Transmission electron microscopy (TEM) was performed on a JEOL 2011 operation at 200 kV. X-ray diffraction (XRD) patterns were recorded on a Rigaku X-ray diffractometer D/MAX-2200/PC equipped with Cu *Kα* radiation (40 kV, 20 mA). X-ray photoelectron spectroscopy (XPS) results were obtained with PHI 5000C ESCA with Mg *Kα* source operating at 14 kV and 25 mA. UV–vis diffuse reflectance spectroscopy was performed in triplicate on similar samples to ensure reproducibility, on a SHIMADZU UV-2450 with a collection speed of 40 nm min^{-1} and $BaSO_4$ as the reference. All samples were obtained by scratching films off the FTO substrates and degassing at 200 °C overnight.

Prior to irradiation, 12 fabricated DSPC cells (the volume of each cell was 12.5 mL) were fixed vertically into an oscillation box, and were simultaneously shaken in the dark, for 40 min, to establish adsorption–desorption equilibrium of the solution species with the electrodes. Then water samples for analysis were taken when all 12 cells were irradiated for two hours using an AM 1.5 solar simulator (Oriel) equipped with a 150 W xenon light and AM 1.5G type filter (Newport, 81094). It should be noted that samples for analyses were collected at 10-min interval sequentially from ordered DSPCs (*e.g.* sample #1 was collected from cell #1 at $t = 0$, sample #2 was collected from cell #2 at $t = 10$ min, etc.) since the liquid volume in each cell was small and repeated sampling only from one cell would have interfered with the cell performance. The current–voltage (*J–V*) characteristics of the 12 cells were measured as described elsewhere [24]. The amount of hydrogen, the concentrations of EE2, TOC, TN and DO were measured as shown in our previous studies [4,14,25]. Briefly, the concentration of EE2 was detected by high performance liquid chromatography (HPLC, Agilent 1100). TOC was measured by means of a Shimadzu TOC-V_{VPN} with an ANSI-V auto sampler. TN was measured using multi N/C 2100 TOC analyzer (Analytikjena, Germany). DO was monitored with electrode for DO sensor (UC-12-SOL, Central Kagaku Co.). The gas produced was collected by the water displacement method using a solution containing sulfuric acid (2%) and NaCl (10%) and then measured using a gas chromatograph (HP Agilent, 6890) equipped with a thermal conductivity detector and a molecular sieve 5A column.

3. Results and discussion

3.1. Characterization of Ag/AgCl @ chiral TiO_2 nanofibers

SEM pictures of the Ag/AgCl @ chiral TiO_2 nanofibers (Fig. 2a) revealed that the left-handed, double-helical morphology was preserved after the deposition of the Ag and AgCl nanoparticles. The average length of undamaged TiO_2 nanofibers was ~500 nm and diameter was ~20 nm. TEM analyses (Fig. 2b–c) revealed that Ag/AgCl nanoparticles with the average diameters of 5–8 nm were deposited on the surface of the chiral TiO_2 nanofibers, preferentially at the outer edges of the TiO_2 crystals of the helical structure, following the conceptual structure shown in Fig. 2d.

The elemental and chemical compositions of the samples were further determined by XPS. The results (Fig. S1a, Supplementary Material) suggest that Ag/AgCl @ chiral TiO_2 nanofibers contain Ti, O, C, Ag and Cl elements. The C1s was attributed to the adventitious hydrocarbon released from the XPS instrument [23]. In Fig. S1b (Supplementary Material), the Ag 3d spectra consists of two individual peaks approximately at 373 and 367 eV, which are due to Ag $3d_{3/2}$ and Ag $3d_{5/2}$ binding energy, respectively. The existence of Ag^0 and Ag^{+1} could be verified by further peaks divisions [24]. Consequently, the XPS analyses suggested that the nanoparticles deposited on chiral TiO_2 nanofibers were made of Ag/AgCl composites. The elemental composition determined by EDX (Fig. S2, Supplementary Material), resulted in a Ag content of 5.49 mol % and a Cl content of 2.86 mol %, which indicated that the Ag/AgCl was virtually at a 1:1 molar ratio. XRD results also suggested the co-existence of Ag and AgCl (Fig. S3 and detailed descriptions in Supplementary Material). Further details on material characterization have been reported [22]. Moreover, the chiral nanostructure was preserved after the doctor-blade process although some aggregation of the nanofibers was observed (Fig. 3).

3.2. Contaminants removal in the DSPC

EE2 representing for chemically stable organic compounds and Cu^{2+} representing for heavy metal ions were spiked into the wastewater at specific concentrations to investigate the removal of contaminants (TOC, TN, EE2 and Cu^{2+}) in the cell (Fig. 4). TOC, Cu^{2+} and EE2 were totally removed after 80 min, while only approximately 70% of TN was removed within 120 min. Simultaneously, a decrease of DO over time was observed, suggesting that the mineralization of TOC and EE2 was aerobic [15]. The fast photodegradation of the TOC including EE2 should be attributed to the combined effect of (i) the strong photocatalytic activity of irradiated Ag/AgCl @ chiral TiO_2 nanofibers and of (ii) the oxidization ability of sensitized dyes. Regarding the first effect, Ag/AgCl @ chiral TiO_2 nanofibers under visible-light irradiation produces photogenerated electron-hole pairs in the Ag nanoparticles due to surface plasmon resonance (SPR) [26]. In this process, SPR generates the electron–hole pairs in the semiconductor (AgCl and TiO_2) by the dipole–dipole interaction between the donor (Ag) and the acceptors (AgCl and TiO_2). The photocatalytic activity of Ag/AgCl @ chiral TiO_2 nanofibers should mainly be attributed to two simultaneous processes. The first process involves the strong electronic coupling between Ag and AgCl conduction bands, which injects photoinduced electrons from the Ag nanoparticles, quickly and efficiently, into the AgCl [27] and into the TiO_2 helical structure, probably yielding superoxide radicals and finally HO· radicals from the reductive pathway, as reported with other dyes [28]. However, this effect should not be significant for the removal of the contaminants since the direct charge transfer from the noble nanoparticles, or the internal photoemission from TiO_2 and

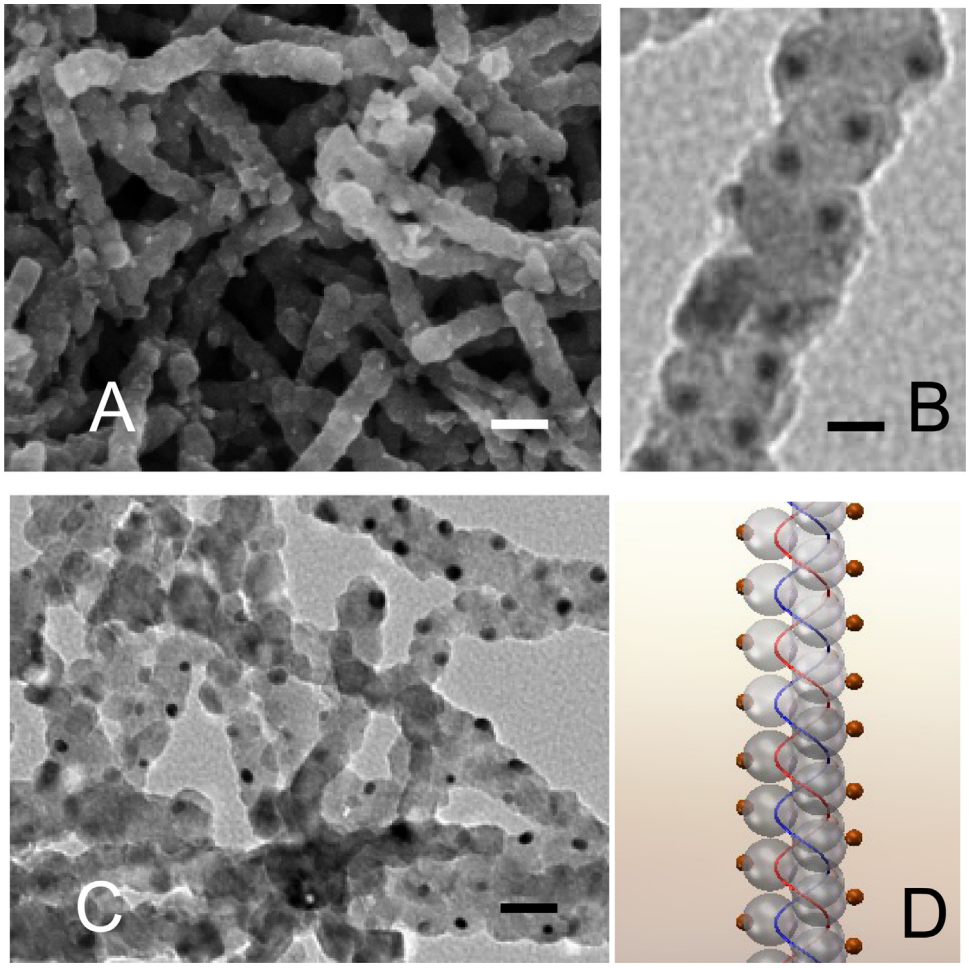

Fig. 2. Microscopy and schematic drawing of Ag/AgCl @ chiral TiO_2 nanofibers. (A) SEM image of Ag/AgCl @ chiral TiO_2 nanofibers. (B, C) TEM images of Ag/AgCl @ chiral TiO_2 nanofibers, which shows the nanoparticles deposited on the surfaces of Ag/AgCl @ chiral TiO_2 nanofibers. (D) Structural model showing Ag/AgCl nanoparticles deposited on the double helixes. The scale bars in A, B and C represent 40, 10 and 20 nm, respectively.

AgCl [29], only plays a supporting role in the photoelectrical performance. This was verified of the *J–V* characteristics of the solar cells not sensitized without dye N719 (see Fig. S5, Supplementary Material).

Regarding the effect of the sensitized dye on the removal of TOC and EE2, the redox potential of N719/sensitized N719 is ~1.1 V (*vs.* normal hydrogen electrode (NHE)) [21] and sensitized N719/oxidized N719 is ~−0.6 V (*vs.* NHE) [30] which is sufficient to oxidize most organic compounds in wastewater, since their redox potentials were mostly less than 0.6 V *vs.* NHE [31]. As a result, the reduction of the sensitized dye to its ground state maintained the cell cycle until all organic contaminants were removed from the wastewater. Since the pH of the wastewater in the cell was

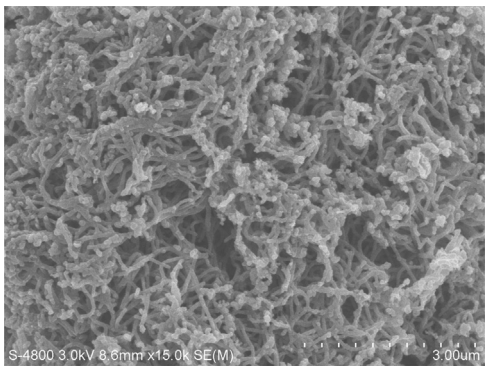

Fig. 3. SEM image of the photoanode film after deposition by the doctor-blade process and calcination.

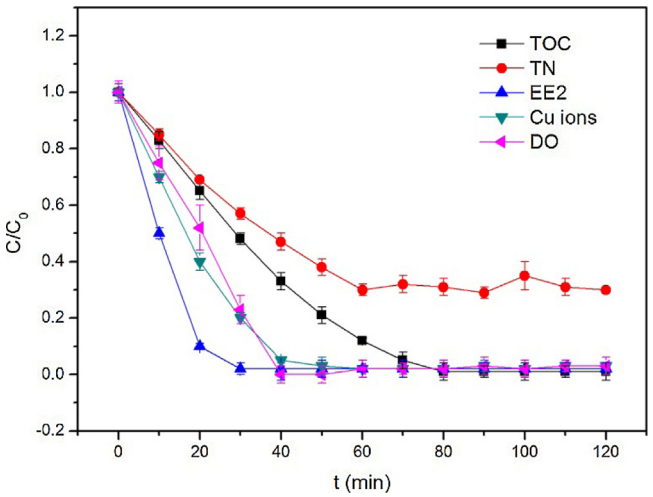

Fig. 4. The removal of contaminants in the cell. The initial concentrations of TOC, EE2, DO and TN were 44 mg/L, 0.56 mg/L, 6.7 mg/L and 13 mg/L, respectively. The pH of wastewater was adjusted to 6.0.

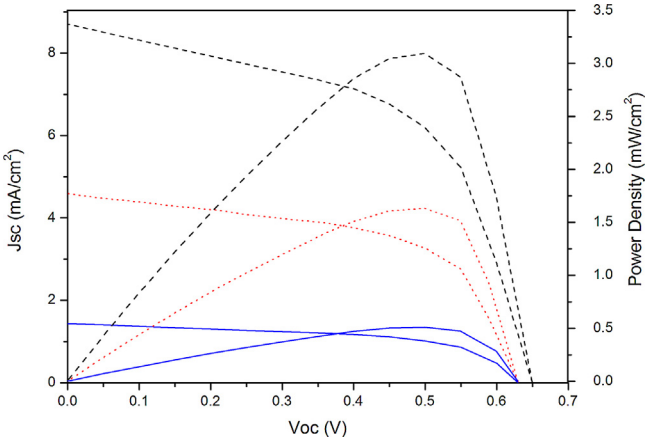

Fig. 5. The electrical performance of the cell: 0 min (black dash trace), 40 min (red dot trace) and 70 min (blue solid trace). The pH of wastewater was adjusted to 6.0. (For interpretation of the references to color in this figure legend, the reader is referred to the web version of this article.)

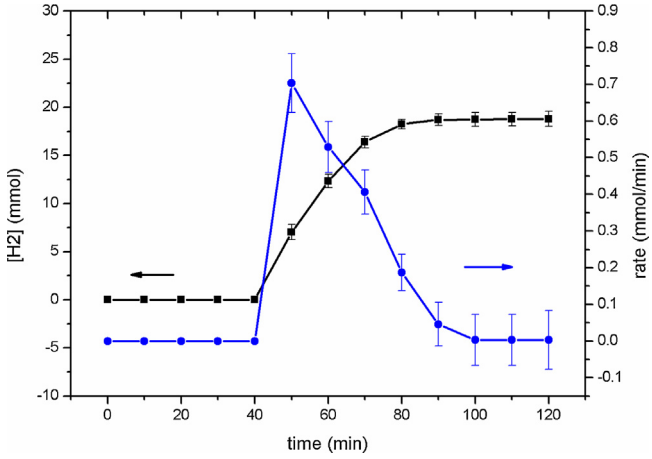

Fig. 6. The accumulation of H_2 in the cell (■) and the rate of H_2 production (•). The pH of wastewater was adjusted to 6.0.

slightly acidic, the decrease in the TN should be attributed to the reduction of NO_3^- of the wastewater by the electrons transferred to the photocathode:

$$2NO_3^- + 10H^+ + 8e^- \rightarrow N_2O + 5H_2O \quad E^0 = 0.7989\,V \tag{1}$$

$$NO_3^- + 4H^+ + 3e^- \rightarrow NO + 2H_2O \quad E^0 = 0.9637\,V \tag{2}$$

This significant mass deficit in the TN balance also confirms that some gaseous product such as NO and N_2O were generated as a result of NO_3^- reduction. The residual 30% of TN remaining after the photoelectrical degradation of contaminants was completed should be in the form of NH_3-N as it could not be reduced in either acidic or neutral conditions [32].

3.3. Photoelectrical performance and hydrogen generation of the DSPC

SPR is characterized by a build-up of intense, spatially non-homogeneous oscillating electric fields in the neighborhood of the nanostructure [22]. The SPR effect at the photoanode improves the efficiency of the DSPCs by (1) increasing light absorption due to surface plasmons and light-trapping effects, (2) facilitating the charge separation as a result of the localized electro-magnetic field, (3) promoting the electron transfer to the adsorbed species, and (4) as a result of the electron storage effect that can shifts the Fermi level to more negative potentials [33–36]. Although the direct charge transfer from Ag nanoparticles to the semiconductor may also prove useful for the generation of electricity as mentioned above, the main mechanism of photo-excitation of the photoanode with visible light implies the sensitization of the N719 dye, and the transfer of excited electrons to the Ag/AgCl @ chiral TiO_2 nanofibers, the external load, the counter cathode and lastly the simultaneous reductions of NO_3^-, H^+ and Cu^{2+}. The presence of metallic Cu on the surface of the counter electrode after the reduction process was further substantiated by two XPS peaks at 932.6 eV and 952.5 eV (Fig. S4, Supplementary Material). In parallel to the above mechanism, the sensitized N719 dye is reduced back to its ground state by the adsorbed organic matter and nitrogen, which were present in the wastewater, making sacrificial organic and inorganic matter essential to sustain the mechanism of the DSPCs. This mechanism is further exemplified by the current–voltage (J–V) and current–power densities (J–P) plots, which were recorded to investigate the electrical performance of the cell (Fig. 5). The short-circuit current densities (J_{sc}), open-circuit voltage (V_{oc}) and power densities varied with time during the irradiation of the DSPCs. J_{sc} decreased significantly over time and it even turned to be 0.02 mA/cm^2 after 80 min and then remained stable, while V_{oc} decreased moderately (Table S2, Supplementary Material). These should be attributed to the removal of contaminants in the cell as they functioned as electrons bridges. Moreover, J_{sc} is determined by electron injection [20,35] which depends on the concentration of contaminants, hence, J_{sc} decreased eventually to a relatively low level as the contaminants were totally removed, after 80 min. However, J_{sc} did not decrease to 0 as expected, since Ag can also be excited by visible-light irradiation while TiO_2 can be excited by the small fraction of UV accessible under AM 1.5 irradiation, which produced electron–hole pairs [33]. Then the produced electrons transferred through the external load to the cathode while the holes may react with H_2O. This is consistent with the photoelectrical performance of the solar cells not sensitized with N719 (Fig. S5, Supplementary Material). In addition, these produced holes may also oxidize some N719 molecules and disable the DSPC (this will be discussed in following section). In contrast, V_{oc} is largely affected by the properties of the photoanode, *i.e.*, the conductive band potential of the photoanode and the dye absorption number [36], thus V_{oc} decreased.

The characterization of the cell under dark conditions is shown in Fig. S6 (Supplementary Material). The dark currents observed due to the presence of $CuSO_4$ (J_{sc} of 0.016 mA/cm^2) were insignificant in comparison with the currents observed under irradiation (Fig. 5). Cu^{2+} is practically removed from the aqueous solution in 40 min (Fig. 4) to which corresponds a J_{sc} of 4.59 mA/cm^2.

The fill factors (Table S2, Supplementary Material) were calculated according to [16,37]:

$$ff = \frac{P_{max}}{J_{sc}V_{oc}} \tag{3}$$

where P_{max} is the maximum power density.

Fig. 6 shows the photogeneration of H_2 over time in the DSPCs. The electrons transferred to the counter electrode reduced protons to H_2, although some H_2 could also be formed during the degradation of organic matter [11,38]. The accumulation of H_2 was not observed until 40 min *ca.*, when DO and Cu^{2+} were almost totally consumed (Fig. 4) as the redox potentials of Cu^{2+}/Cu (0.3394 V *vs.* NHE) and the redox potentials of O_2/H_2O (1.229 V *vs.* NHE) were higher than that of H^+/H_2 (0 *vs.* NHE) [39]. In agreement with the electrical performance, the rate of H_2 production gradually decreased as the concentration of contaminants decreased and reached approximately zero, after 80 min, when the electricity was only generated due to the excitation of TiO_2 and Ag under irradiation.

The photo-electricity conversion efficiency (PCE) was calculated (Table S2, Supplementary Material) to evaluate the photoelectrical performance of the DSPC. An efficiency of 3.09% was recorded at 0 min, indicating 3.09% of the incident light energy was converted into electricity. Moreover, the electricity–hydrogen conversion efficiency (ECE) was calculated:

$$ECE(\%) = \frac{E_{H_2}}{E_{el}} = \frac{2n_t U}{\int P_{max} A dt} \times 100 \quad (4)$$

where E_{H_2} is the H_2 energy (J) produced by the cell, E_{el} is the generated electrical energy on the photoanode (J), P_{max} is the maximum power density (W/cm^2), A is the irradiated surface area of photoanode (cm^2), n is the total amount of hydrogen produced (mol), U is the hydrogen energy content (122 kJ/g) and t is time (s). As shown in Table S2, 78.1% of the electricity generated from 40 to 50 min was converted to hydrogen energy. While after 60 min, approximately 98% of the electricity was converted due to the total removal of NO_3^- in the wastewater.

3.4. Chirality and plasmonic effect in the DSPC

The highest PCE in this study was 3.09% which is relatively high considering that the electrolyte was actual wastewater rather than I^-/I_3^- solution. This supports the superior performance of Ag/AgCl @ chiral TiO_2 nanofibers as photoanode in the DSPC. Herein, the photoanodes prepared with chiral TiO_2 nanofibers, Ag/AgCl @ broken chiral TiO_2 nanofibers served as controls, to exemplify the chiral plasmonic effect on the performance of the DSPC. The SEM and TEM pictures of these reference photoanode are shown in Fig. S7 (Supplementary Material). The absorption spectrums of Ag/AgCl @ chiral TiO_2 nanofibers thin film and other reference photoanode thin films are shown in Fig. S8 (Supplementary Material). The stronger absorption of Ag/AgCl @ chiral TiO_2 nanofibers at 200–350 nm compared to pure chiral TiO_2 nanofibers can be attributed to the characteristic absorption of the AgCl semiconductor [40], besides, Ag NPs can absorb photons from an area much larger than their geometric cross section. Resonance energy transfer (RET), the transfer of energy from a plasmon to a nearby semiconductor, enhances the intensity of the electric field thereby increasing optical absorption [41]. In contrast, the increased response in the visible-light region (400–800 nm) results from the creation of SPR [42]. The significant red shift of the absorption edge observed in the Ag/AgCl @ chiral TiO_2 nanofibers (trace c) when compared with Ag/AgCl @ broken chiral TiO_2 nanofibers (trace b), demonstrates that controlled chirality at the nanoscale level combined with the periodic distribution of the plasmonic Ag/AgCl in the chiral TiO_2 nanofiber, induces a greater SPR effect. The nanostructured ordered helical arrangement of the Ag/AgCl nanoparticles induces coupled plasmon waves propagating along the helical path, causing increased absorption of the incident light components that are in tune with the handedness of the helices. The collective plasmons that oscillate along the plasmonic chiral structure of certain handedness lead to different rate of light absorption in response to right- and left-circularly polarized light [42]. Therefore, the acceleration of SPR excitation results from the nanostructured architecture of ordered and periodically positioned Ag/AgCl nanoparticles (Fig. 2), which are irradiated at specific incident polarization angles. Thus, it could be concluded that the more intense SPR created by Ag nanoparticles of Ag/AgCl @ chiral TiO_2 nanofibers can cause a stronger local field enhancement around the Ag nanoparticles, which can increase light absorption of the surrounding dye molecules in a dye-loaded film (Fig. S8, Supplementary Material). The higher rate of light absorption by the dye can result in an enhancement of the rate of electron injection to the photoanode [43].

The production of energy of the DSPC with the Ag/AgCl @ chiral TiO_2 nanofibers photoanode and with other reference photoanodes were also studied (Fig. S9, Supplementary Material) to exemplify the advantages associated with the use of a chiral plasmonic structure. The PCE values of the cell with Ag/AgCl @ chiral TiO_2 nanofibers photoanode were higher than those of the reference cell with Ag/AgCl @ broken chiral TiO_2 nanofibers, which should be partly attributed to the higher light harvesting efficiency of the unbroken nanofibers. Furthermore, in these materials Ag nanoparticles act as an effective 'antenna' for the incident visible light that stores the incident energy and create an intense electromagnetic field in the immediate vicinity [33], which in turn increases the rate of electron–hole formation in some localized regions of the semiconductor by a few orders of magnitude [43]. Concurrently, nanofibers owns faster electron transport, slower recombination rate [44,45] and can serve as light-scattering centers to increase the optical light extinction length in the film, thus also enhancing the light harvesting efficiency [24]. Hence, in the photoanode of this cell, chiral TiO_2 nanofibers and Ag nanoparticles act in a symbiotic relationship that improves the electrical performance of Ag/AgCl @ chiral TiO_2 nanofibers film. Firstly, the SPR effect of Ag nanoparticles is accelerated by the chiral structure due to its capacity of tuning the angle of the incident light and the scattering of light. Secondly, the lifetime of the large amount of electrons generated is extended, owning to the faster electron transport and slower recombination rate in the chiral TiO_2 nanofibers. Thirdly, the surface plasmons and light scattering (Ag also acts as a scattering center) can increase the intensity of the local field and light pathways, which enlarges the optical cross-section of dye sensitizer coated on the photoanode [46]. However, it was unexpected that only a slightly higher PCE of the cell with Ag/AgCl @ chiral TiO_2 nanofibers was observed in comparison to the PCE of pure chiral TiO_2 nanofibers (Fig. S9, Supplementary Material). We reason that this is due to the Ag nanoparticles acting as recombination centers, in essence creating internal short-circuits throughout the bulk of the photoactive layer [47]. Hence, the slight PCE improvement should be ascribed to the trade-off between the chiral plasmonic effect and the electron recombination role of Ag nanoparticles.

3.5. Cell stability and reuse

The stability and reuse of the DSPC was investigated to establish the effect of inactivation caused by the leaching of dye from the photoanode or by the deposition of by-products on the electrodes. Fig. 7 shows the absorbance of N719 dye deposited on the photoanode as a function of time t relative to the absorbance of a freshly prepared photoanode (*i.e.*, A_t/A_0) [48]. 45% of the dye was found to desorb after 24 h immersion in wastewater, while only 20% of the dye remained after 120 h. Therefore, with such long timescale the reduction of photoelectrical performance shown in Fig. 5 cannot be attributed to dye detachment alone.

In general, water is believed to cause a loss of activity in the DSPCs [49,50]. For the particular case of N719 dye, since the redox potential of ROS/H_2O (~2.85 V *vs.* NHE) [28] is higher than that of N719/sensitized N719 (~1.0 V *vs.* NHE) [33] it is conceivable that the leached dye could be oxidized by ROS after the total consumption of TOC from the wastewater.

Such effect was demonstrated by examining the photoanode absorbance and photoelectrical performance of the cell with the wastewater sealed in the cell replaced by fresh wastewater every hour or every two hours (referred as 1 h cell and 2 h cell). The rate of leached dye (Fig. 7) for the 1 h cell was as that with the photoanode immersed in wastewater since the TOC of the wastewater was never totally consumed. In contrast, the rate of leached dye for the 2 h cell was much more rapid, implying that the N719 molecules were oxidized by the excited ROS after the total removal of TOC.

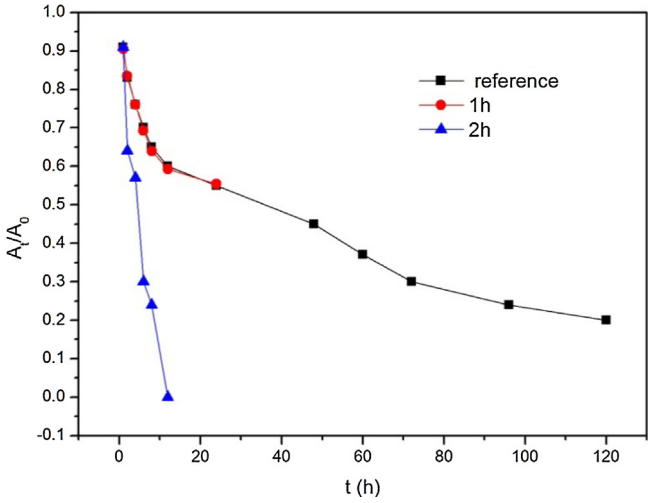

Fig. 7. Relative A_t/A_0 absorbance of dye molecules (at 510 nm) detached from the photoanode immersed in wastewater (■), from the photoanode in the cell with wastewater replaced every hour (•) and every two hours (▲).

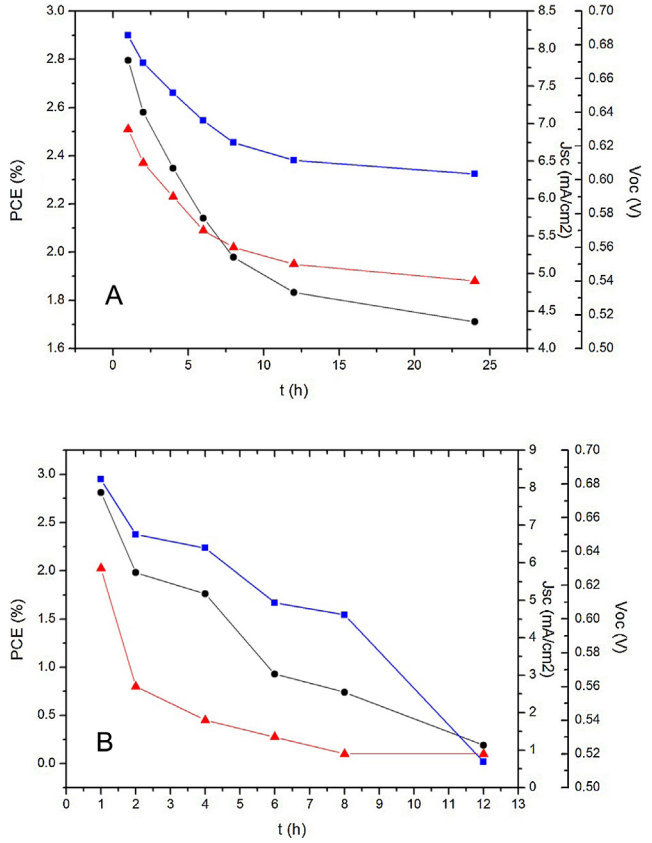

Fig. 8. Time evolution of PCE (•), J_{sc} (■) and V_{oc} (▲) for the cell with the wastewater replaced (A) every hour (referred as 1 h cell) and (B) every two hours (referred as 2 h cell). All data were recorded immediately when the wastewater was replaced with fresh wastewater.

Similarly, the photoelectrical performance of the 1 h cell (Fig. 8) showed PCE values of the 1 h cell decreasing by approximately 50% (mainly due to the lower J_{sc}), and lower V_{oc} after 24 h, which can be ascribed to dye desorption [20]. However, the loss of photoelectrical performance was significantly higher for the 2 h cell with a 90% decrease of the PCE after 12 h, which should be attributed to the oxidization of N719 after the removal of TOC of the wastewater. Therefore, a more stable performance of the photoanodes can be anticipated if the cell was operated with a continuous flow of fresh wastewater. Further research efforts should be directed toward the production of more stable dyes for use in water-based DSPCs including the use of electrolyte additives (such as ionic surfactants) [51–55] and the use of hydrophobic dye sensitizers [49].

4. Conclusion

In summary, a DSPC with Ag/AgCl @ chiral TiO_2 nanofibers as photoanode material, platinized conducting glass as cathode material and actual wastewater as the bridging electrolyte was proposed for simultaneous generation of electricity, hydrogen and contaminants removal. Excellent photoelectrical performance, fast hydrogen generation and contaminants removal were observed due to the symbiotic relationship between Ag nanoparticles and chiral nanofibers, which was exemplified by comparing the photoelectrical performance of Ag/AgCl @ chiral TiO_2 nanofibers photoanode with that of Ag/AgCl @ broken chiral TiO_2 nanofibers. This configuration opens up new opportunities for producing renewable energy from wastewater treatment processes including organic and inorganic matter as viable resources. Chiral nanofibers doped with SPR metal nanoparticles photoanode have great potential in boosting the performance of DSPC. Although the novel DSPC shown here is far from optimum performance, there are huge opportunities for further development. The introduction of a semiconductor insulator could hinder Ag from capturing electrons and the operation of the cell in continuous flow of wastewater may reduce dye leaching. With continued advances in DSPCs for water-based applications, it may therefore be possible to increase the efficiency of energy generation and contaminants removal and finally achieve its successful implementation in domestic and industrial wastewater treatment processes.

Acknowledgements

The study was financially supported by the National Natural Science Foundation of China (No. 51322901 and No. 51479066), the Foundation for Innovative Research Groups of the National Natural Science Foundation of China (51421006) and the Fundamental Research Funds for the Central Universities (No. 2014B02914 and 2014B39514).

Appendix A. Supplementary data

Supplementary data associated with this article can be found, in the online version, at http://dx.doi.org/10.1016/j.apcatb.2014.11.012.

References

[1] P.L. Mcarty, J. Bae, J. Kim, Domestic wastewater treatment as a net energy producer – can this be achieved? Environ. Sci. Technol. 45 (2011) 7100–7106.
[2] H. Liu, B.E. Logan, Electricity generation using an air-cathode single chamber microbial fuel cell in the presence and absence of a proton exchange membrane, Environ. Sci. Technol. 38 (2004) 4040–4046.
[3] S.K. Chaudhuri, D.R. Lovley, Electricity generation by direct oxidation of glucose in mediatorless microbial fuel cells, Nat. Biotechnol. 21 (2003) 1229–1232.
[4] D. Wang, Y. Li, W. Zhang, Q. Wang, C. Wang, P. Wang, Development and modeling of a flat plate serpentine reactor for photocatalytic degradation of 17-ethinylestradiol, Environ. Sci. Pollut. Res. 20 (2013) 2321–2329.
[5] M. Narumiya, N. Nakada, N. Yamashita, H.H. Tanaka, Phase distribution and removal of pharmaceuticals and personal care products during anaerobic sludge digestion, J. Hazard. Mater. 260 (2013) 305–312.
[6] J. Shen, C. Ou, Z. Zhou, J. Chen, H. Fang, X. Sun, J. Li, L. Zhou, L. Wang, Pretreatment of 2,4-dinitroanisole (DNAN) producing wastewater using a combined zero-valent iron (ZVI) reduction and Fenton oxidation process, J. Hazard. Mater. 260 (2013) 993–1000.
[7] S. Papadimitriou, S. Armyanov, E. Valova, A. Hubin, O. Steenhat, E. Pavlidou, G. Kokkinidis, S. Sotiropoulos, Methanol oxidation at Pt–Cu, Pt–Ni, and Pt–Co

electrode coatings prepared by a galvanic replacement process, J. Phys. Chem. C 114 (2010) 5217–5223.
[8] V.K. Gupta, R. Jain, A. Mittal, T.A. Saleh, A. Nayak, S. Agarwal, S. Sikarwar, Photocatalytic degradation of toxic dye amaranth on TiO_2/UV in aqueous suspensions, Mater. Sci. Eng. C 32 (2012) 12–17.
[9] D.M.A. Alrousan, M.I. Polo-Lopez, P.S.M. Dunlop, P. Fernandez-Ibanez, J.A. Byrne, Solar photocatalytic disinfection of water with immobilised titanium dioxide in re-circulating flow CPC reactors, Appl. Catal. B: Environ. 128 (2012) 126–134.
[10] M.N. Chong, B. Jin, C.W.K. Chow, C. Saint, Recent development in photocatalytic water treatment technology: a review, Water Res. 44 (2010) 2997–3027.
[11] J. Kim, W.W. Choi, Hydrogen producing water treatment through solar photocatalysis, Energy Environ. Sci. 3 (2010) 1042–1045.
[12] J. Kim, D. Monllor-Satoca, W. Choi, Simultaneous production of hydrogen with the degradation of organic pollutants using TiO_2 photocatalyst modified with dual surface components, Energy Environ. Sci. 5 (2012) 7647–7656.
[13] K. Li, Y. Xu, Y. He, C. Yang, Y. Wang, J.J. Jia, Photocatalytic fuel cell (PFC) and dye self-photosensitization photocatalytic fuel cell (DSPFC) with BiOCl/Ti photoanode under UV and visible light irradiation, Environ. Sci. Technol. 47 (2013) 3490–3497.
[14] W. Zhang, Y. Li, C. Wang, P. Wang, Q. Wang, Energy recovery during advanced wastewater treatment: simultaneous estrogenic activity removal and hydrogen production through solar photocatalysis, Water Res. 47 (2013) 1480–1490.
[15] W. Zhang, Y. Li, C. Wang, P. Wang, Q. Wang, D. Wang, Mechanisms of simultaneous hydrogen production and estrogenic activity removal from secondary effluent through solar photocatalysis, Water Res. 47 (2013) 3173–3182.
[16] P. Lianos, Production of electricity and hydrogen by photocatalytic degradation of organic wastes in a photoelectrochemical cell. The concept of the PhotoFuelCell: a review of a re-emerging research field, J. Hazard. Mater. 185 (2011) 575–590.
[17] E. Stathatos, P. Lianos, S.M. Zakeeruddin, P. Liska, M. Grätzel, A Quasi-solid-state dye-sensitized solar cell based on a sol–gel nanocomposite electrolyte containing ionic liquid, Chem. Mater. 15 (2003) 1825–1829.
[18] E. Stathatos, P. Lianos, U. Lavrencic-Stangar, B. Orel, A high-performance solid-state dye-sensitized photoelectrochemical cell employing a nanocomposite gel electrolyte made by the sol–gel route, Adv. Mater. 14 (2002) 354–357.
[19] M. Antoniadou, P. Lianos, Production of electricity by photoelectrochemical oxidation of ethanol in a PhotoFuelCell, Appl. Catal. B: Environ. 99 (2010) 307–313.
[20] Z. Ning, Y. Fu, H. Tian, Improvement of dye-sensitized solar cells: what we know and what we need to know, Energy Environ. Sci. 3 (2010) 1170–1181.
[21] F. Hao, P. Dong, Q. Luo, J. Li, J. Lou, H. Lin, Recent advances in alternative cathode materials for iodine-free dye-sensitized solar cell, Energy Environ. Sci. 6 (2013) 2003–2019.
[22] D. Wang, Y. Li, G. Li Puma, C. Wang, P. Wang, W. Zhang, Q. Wang, Visible-light driven plasmon photocatalyst Ag/AgCl@helical chiral TiO_2 nanofibers, Chem. Commun. 49 (2013) 10367–10369.
[23] A. Mills, N. Elliott, G. Hill, D. Fallis, J.R. Durrant, R.L. Willis, Preparation and characterization of novel thick sol–gel titania film photocatalysts, Photochem. Photobiol. Sci. 2 (2003) 591–596.
[24] Y. Bai, H. Yu, Z. Li, R. Amal, G.Q. Lu, L. Wang, In situ growth of a ZnO nanowire network within a TiO_2 nanoparticles film for enhanced dye-sensitized solar cells, Adv. Mater. 24 (2012) 5850–5856.
[25] D. Wang, Y. Li, G. Li, C. Wang, W. Zhang, Q. Wang, Modeling of quantitative effects of water components on the photocatalytic degradation of 17 α-ethynylestradiol in a modified flat plate serpentine reactor, J. Hazard. Mater. 254–255 (254) (2013) 64–70.
[26] J. Yu, G. Dai, B. Huang, Fabrication and characterization of visible-light driven plasmonic photocatalyst Ag/AgCl/TiO_2 nanotube arrays, J. Phys. Chem. C 113 (2009) 16394–16401.
[27] Y. Tang, Z. Jiang, G. Xing, A. Li, P.D. Kanhere, Y. Zhang, T.C. Sum, S. Li, X. Chen, Z. Dong, Z. Chen, Efficient Ag@AgCl cubic cage photocatalysts profit from ultrafast plasmon-induced electron transfer processes, Adv. Funct. Mater. 23 (2013) 2932–2940.
[28] T.X. Wu, G.M. Liu, J.C. Zhao, H. Hidaka, N. Serpone, Photoassisted degradation of dye pollutants. V. Self-photosensitized oxidative transformation of rhodamine B under visible light irradiation in aqueous TiO_2 dispersions, J. Phys. Chem. B 102 (1998) 5845–5851.
[29] C. Hagglund, M. Zach, B. Kasemo, Enhanced charge carrier generation in dye-sensitized solar cells by nanoparticles plasmons, Appl. Phys. Lett. 92 (2008) 013113.
[30] T. Daeneke, T.-H. Kwon, A.B. Holmes, N.W. Duffy, U. Bach, L. Spiccia, High-efficiency dye-sensitized solar cells with ferrocene-base electrolytes, Nat. Chem. 3 (2011) 211–215.
[31] D.T. Scott, D.M. McKnight, E.L. Blunt-Harris, S.E.D.R. Kolesar, Lovely quinone moieties act as electron acceptors in the reduction of humic substances by humics-reducing microorganisms, Environ. Sci. Technol. 32 (1998) 2984–2989.
[32] J. Lee, H. Park, W. Choi, Selective photocatalytic oxidation of NH_3 to N_2 on platinized TiO_2 in water, Environ. Sci. Technol. 36 (2002) 5462–5468.
[33] H. Choi, W.T. Chen, P.V. Kamat, Know thy nanoneighbor. Plasmonic versus electron charging effects of metal nanoparticles in dye-sensitized solar cell, ACS Nano 6 (2012) 4418–4427.
[34] D. Bui, J. Mu, L. Wang, S. Kang, X. Li, Preparation of Cu-loaded $SrTiO_3$ nanoparticles and their photocatalytic activity for hydrogen evolution from methanol aqueous solution, Appl. Surf. Sci. 274 (2013) 328–333.
[35] T. Marinado, K. Nonomura, J. Nissfolk, M.K. Karlsson, D.P. Hagberg, L. Sun, S. Mori, A. Hagfeldt, How the nature of triphenylamine–polyene dyes in dye-sensitized solar cells affects the open-circuit voltage and electron lifetimes, Langmuir 26 (2009) 2592–2598.
[36] B.C. O'Regan, J.R. Durrant, Kinetic and energetic paradigms for dye-sensitized solar cells: moving from the ideal to the real, Acc. Chem. Res. 42 (2009) 1799–1808.
[37] B.C. O'Regan, M. Gratzel, Low-cost, high-efficiency solar cell based on dye-sensitized colloidal TiO_2 films, Nature 24 (1991) 737–740.
[38] H.C. Park, D. Vecitis, W. Choi, O. Weres, M.R. Hoffmann, Solar-powered production of molecular hydrogen from water, J. Phys. Chem. C 112 (2008) 885–889.
[39] J.A. Dean, Lange's Handbook of Chemistry, 15th ed., McGraw-Hill Professional, 1998.
[40] P. Wang, B. Huang, Z. Lou, X. Zhang, X. Qin, Y. Dai, Z. Zheng, X. Wang, Synthesis of highly efficient Ag@AgCl plasmonic photocatalysts with various structures, Chem. Eur. J. 16 (2010) 538–544.
[41] S.C. Warren, E. Thimsen, Plasmonic solar water splitting, Energy Environ. Sci. 5 (2012) 5133–5146.
[42] X. Shen, C. Shen, J. Wang, D. Shi, Z. Wang, N. Liu, B. Ding, Rolling up gold nanoparticle-dressed DNA origami into three-dimensional plasmonic chiral nanostructures, J. Am. Chem. Soc. 134 (2012) 146–149.
[43] J. Lee, T. Javed, T. Skeini, A.O. Govorov, G.W. Bryant, N.A. Kotov, Bioconjugated Ag nanoparticles and CdTe nanowires: metamaterials with field-enhanced light absorption, Angew. Chem. Int. Ed. 45 (2006) 4819–4823.
[44] J. Liao, B. Lei, D. Kuang, C. Su, Tri-functional hierarchical TiO_2 spheres consisting of anatase nanorods and nanoparticles for high efficiency dye-sensitized solar cells, Energy Environ. Sci. 4 (2011) 4079–4085.
[45] Y. Ohsaki, N. Masaki, T. Kitamura, Y. Wada, T. Okamoto, T. Sekino, K. Niihara, S. Yanagida, Dye-sensitized TiO_2 nanotube solar cells: fabrication and electronic characterization, Phys. Chem. Chem. Phys. 7 (2005) 4157–4163.
[46] B. Ding, B.J. Lee, M. Yang, H.S. Jung, J.-K. Lee, Surface-plasmon assisted energy conversion in dye-sensitized solar cells, Adv. Energy Mater. 1 (2011) 415–421.
[47] M.D. Brown, T. Suteewong, R.S.S. Kumar, V. d'Innocenzo, A. Petrozza, M.M. Lee, U. Wiesner, H.J. Snaith, Plasmonic dye-sensitized solar cells using core–shell metal-insulator nanoparticles, Nano Lett. 11 (2011) 438–445.
[48] H.J. Son, C. Prasittichai, J.E. Mondloch, L. Luo, J.K.D.W. Wu, O.K. Farha, J.T. Hupp, Dye stabilization and enhanced photoelectrode wettability in water-based dye-sensitized solar cells through post-assembly atomic layer deposition of TiO_2, J. Am. Chem. Soc. 135 (2013) 11529–11532.
[49] C. Law, S.C. Pathirana, X. Li, A.Y. Anderson, P.R.F. Barnes, A. Listorti, T.H. Ghaddar, B.C. O'Regan, Water-based electrolytes for dye-sensitized solar cell, Adv. Mater. 22 (2010) 4505–4509.
[50] Y. Liu, A. Hagfeldt, X.R. Xiao, S.E. Lindquist, Investigation of influence of redox species on the interfacial energetics of a dye-sensitized nanoporous TiO_2 solar cell, Solar Energy Mater. Solar Cells 55 (1998) 267–281.
[51] H. Zhang, L. Qiu, X. Dan, W. Zhang, F. Yan, Performance enhancement of water based dye-sensitized solar cells via addition of ionic surfactants, J. Mater. Chem. 2 (2014) 2221–2226.
[52] T. Daeneke, Y. Uemura, N.W. Duffy, A.J. Mozer, N. Koumura, U. Bach, L. Spiccia, Aqueous dye-sensitized solar cell electrolytes based on the ferricyanide–ferrocyanide redox couple, Adv. Mater. 14 (2012) 1222–1225.
[53] Y. Jung, B. Yoo, M.K. Lim, S.Y. Lee, K.J. Kim, Effect of triton-X in water-added electrolytes on the performance of dye-sensitized solar cells, Electrochim. Acta 54 (2009) 6286–6291.
[54] C. Lian, D. Zhi, S. Xu, H. Liu, Y. Hu, A lattice model for thermally-sensitive core–shell hydrogels, J. Colloid Interface Sci. 406 (2013) 148–153.
[55] C. Lian, L. Wang, X. Chen, X. Han, S. Zhao, H. Liu, Y. Hu, Modeling swelling behavior of thermoresponsive polymer brush with lattice density functional theory, Langmuir 30 (2014) 4040–4048.